Polymer-Stabilized Chromonic Liquid-Crystalline Polarizer

Seul-Ki Park, So-Eun Kim, Dae-Yoon Kim, Shin-Woong Kang, Seunghan Shin, Shiao-Wei Kuo, Seok-Ho Hwang, Seung Hee Lee, Myong-Hoon Lee, and Kwang-Un Jeong**

Robust coatable polarizer is fabricated by the self-assembly of lyotropic chromonic liquid crystals and subsequent photo-polymerizing processes. Their molecular packing structures and optical behaviors are investigated by the combined techniques of microscopy, scattering and spectroscopy. To stabilize the oriented Sunset Yellow FCF (H-SY) films and to minimize the possible defects generated during and after the coating, acrylic acid (AA) is added to the H-SY/H_2O solution and photo-polymerized. Utilizing cross-polarized optical microscopy, phase behaviors of the H-SY/H_2O/AA solution are monitored by varying the compositions and temperatures of the solution. Based on the experimental results of two-dimensional wide angle X-ray diffraction and selected area electron diffraction, the H-SY crystalline unit cell is determined to be a monoclinic structure with the dimensions of $a = 1.70$ nm, $b = 1.78$ nm, $c = 0.68$ nm, $\alpha = \beta = 90.0°$ and $\gamma = 84.5°$. The molecular arrangements in the oriented H-SY films were further confirmed by polarized Fourier-transform infrared spectroscopy. The polymer-stabilized H-SY films show good mechanical and chemical stabilities with a high polarizability. Additionally, patterned polarizers are fabricated by applying a photo-mask during the photo-polymerization of AA, which may open new doors for practical applications in electro-optic devices.

1. Introduction

When a liquid crystalline (LC) phase with long-range molecular- and/or bond-orientational orders in one (1D) or two dimensions (2D) is induced by the addition of a solvent rather than the change of temperature, it is known as a "lyotropic" LC, and is commonly encountered in nature.[1–3] Among various types of lyotropic LCs, lyotropic chromonic LCs (LCLC) have specifically attracted a lot of attention for practical applications as dichroic light-polarizing sheet materials,[4] oriented optical film components,[5,6] and bio-sensing active chemicals,[7] since LCLC can self-assemble into optically and electrically anisotropic films.[8,9]

Generally, LCLC molecules consist of a disk-like rigid core with two or more ionic groups at the periphery of the core.[10–12] At a low concentration, LCLC molecules are dispersed at random without any order. Upon increasing the concentration of the LCLC solution, LCLC molecules spontaneously self-assemble to columns due to the strong π–π interaction between disk-like aromatic cores and the nanophase separation between hydrophobic disk-like core and hydrophilic ionic groups. Therefore, the hydrophilic ionic groups are exposed on the surface of LCLC columns and interact with polar solvent. The lateral size of each LCLC disk is in the order of 1–3 nm and a typical separation between the adjacent LCLC disks along the stacking direction of the column is about 0.34 nm which is an equilibrium distance to maximize the π–π interaction.[2,13,14] It has been known that the aggregation of LCLC occurs even in the isotropic (I) phase. However, the aspect ratio and the volume concentration of columns in the LCLC solution should be high enough to form ordered LC phases. In the columnar nematic (N) phase, LCLC columns aggregate parallel to each other and show a 1D long-range molecular orientational order. When the π–π interaction between disk-like aromatic cores is not strong enough, a common N phase can be formed in an appropriate concentration, which is rarely observed in the lyotropic LC systems.[2,15] LCLC forming N phases can be used in bio-sensing applications due to their biocompatible and non-toxic properties.[16]

S.-K. Park, S.-E. Kim, D.-Y. Kim, Prof. M.-H. Lee, Prof. K.-U. Jeong
Polymer Materials Fusion Research Center and Department of Polymer-Nano Science and Technology
Chonbuk National University
Jeonju 561–756, Korea
E-mail: kujeong@jbnu.ac.kr; mhlee2@chonbuk.ac.kr
Prof. S.-W. Kang, Prof. S. H. Lee
Department of BIN Fusion Technology
Chonbuk National University
Jeonju 561–756, Korea
Dr. S. Shin
Chonan R&D Center
Korea Institute of Industrial Technology
Chonan 330–825, Korea
Prof. S.-W. Kuo
Department of Materials Science and Optoelectronic Engineering
National Sun Yat-Sen University
Kaohsiung 804, Taiwan
Prof. S.-H. Hwang
Department of Polymer Science and Engineering
Dankook University
Yongin 448–701, Korea

DOI: 10.1002/adfm.201002546

© 2011 WILEY-VCH Verlag GmbH & Co. KGaA, Weinheim

At a sufficiently high concentration, the LCLC columns grown with a high aspect ratio self-organize parallel to each other with a quasi-long range positional order perpendicular to the long axis of LCLC columns. This phase can be named as a highly ordered hexagonal/oblique columnar LC phase. If an aqueous solvent is completely evaporated, a crystalline phase can be formed with long-range positional orders in 3D. When the LCLC molecules are oriented at a specific direction, the macroscopically oriented crystalline film can exhibit anisotropic optical and electrical properties.[17–19] Since charge carriers can more effectively travel along the long axis of columns, the oriented LCLC crystalline films exhibit electrical anisotropies and hence can be applied in photovoltaics and electronic devices.[20,21] Moreover, many LCLC materials can absorb light in the visible and near-infrared range because of the aromatic core. Since the molecular orientation in the macroscopically oriented crystalline film is anisotropic, LCLC can be used as E-type polarizing components.[22,23] E-type polarizing film can transmit an extraordinary ray and absorb an ordinary ray, which means that a polarized light traveling perpendicular to the in-plane of LCLC disk (parallel to the long axis of column) can transmit the film. Since the macroscopic molecular orientation can be obtained from the LCLC solution by a simple coating process, the dried LCLC crystalline films can exhibit a significant anisotropy of light absorption, which makes them very attractive for the replacement of the conventional iodine-based external polarizers in the LC display.[24,30] Moreover, the anisotropic LCLC films can work as an alignment layer as well as a polarizer even on the internal flexible substrate, which could offer new possibilities for the development of inexpensive and flexible displays.[30,31] However, despite the various advantages and the growing interest in LCLCs, the practical applications of anisotropic LCLC crystalline films are limited because anisotropic LCLC crystalline films contain a lot of defects (such as cracks) generated during and after coating processes, mainly due to the anisotropic volume shrinkage during crystallization. Additionally, LCLC crystalline films can be attacked by moisture in ambient condition and are fragile against mechanical attacks.

In order to overcome these limitations of anisotropic LCLC crystalline films, we proposed and fabricated the H-Sunset Yellow (H-SY)-based optically anisotropic film which was stabilized via the photo-polymerization of acrylic acid (AA). Phase evolutions of H-SY/H_2O/AA solution were first monitored by varying the compositions of the solution using cross-polarized optical microscopy (POM) and a ternary phase diagram was constructed. The structure, molecular packing symmetry, and morphology were identified using 2D wide-angle X-ray diffraction (WAXD) from the oriented films and were also supported by selected area electron diffractions (SAED). Additionally, the molecular arrangements in the oriented H-SY films were further analyzed by polarized Fourier transform infrared (FT-IR) and polarized ultraviolet-visible (UV–vis) spectroscopies. Bright-field transmission electron microscopy (TEM) images allowed us to confirm that many macroscopic cracks generated in the oriented H-SY films were completely avoided by the photo-polymerization of AA. Utilizing polarized UV–vis spectrometer, optical properties of the oriented H-SY films were evaluated with and without the photo-polymerization of AA. Furthermore, scratch resistance and solubility tests indicated that the mechanical and chemical stabilities of the oriented H-SY films were significantly enhanced by the photo-polymerization of AA.

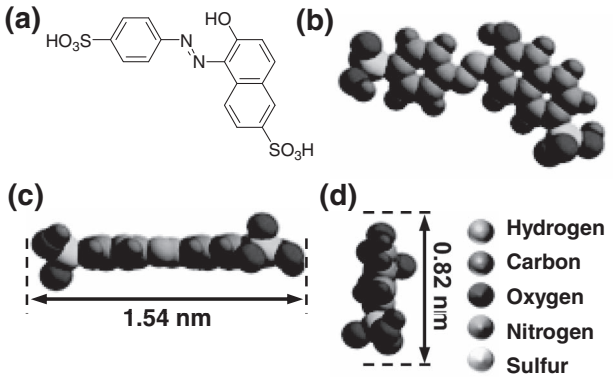

Figure 1. a) Chemical structure of H-SY. Computer energy-minimized geometric dimensions of H-SY in the views from b) front-, c) side-, and d) head directions, respectively.

2. Results and Discussion

2.1. Phase Evolution of H-SY Solutions

Utilizing Cerius^2 computer simulation software from Accelrys, the molecular dimensions and minimal energy geometry of H-SY in the isolated gas phase are first estimated as shown in **Figures 1**b–d: front-, side- and head-views, respectively. The calculated length of H-SY along the long axis is 1.54 nm, while the width of the core is 0.82 nm, as shown in Figures 1c and 1d, respectively. It is worth noting that all the atoms are on the same plane except the oxygen atoms in S=O functions of which long axes are more or less perpendicular to the aromatic core.[2]

POM is employed to study the phase evolutions of H-SY/H_2O and H-SY/H_2O/AA solutions and to construct the phase diagrams with respect to temperature and concentration. Upon varying temperature from 5 to 95 °C and concentration of H-SY in the range of 20–40 wt%, a phase diagram of H-SY/H_2O is constructed as shown in **Figure 2**a. To maintain the original concentration of solutions, the sandwiched LC cells are sealed with epoxy resin prior to POM observations. POM images represented in Figures 2b–e are obtained at room temperature when the concentrations are 25, 30, 35, and 40 wt%, respectively. These concentrations at room temperature form a fan-shaped LC texture, which is one of the typical POM textures of the columnar (Col) LC phase.[32,33] It is worth noting that, upon increasing temperature at a constant concentration or decreasing concentration at a constant temperature, the Col LC phase of H-SY/H_2O transforms a "biphase" of Col LC and isotropic (I) phase before converting completely to the I phase at higher temperatures and at lower concentrations.[1,2,32,33]

Based on the POM observations, a ternary phase diagram of H-SY/H_2O/AA is also built at room temperature by varying the concentration of H-SY/H_2O/AA solutions, as shown in **Figure 3**a. POM textures taken at the different concentrations are also presented in Figures 3b–d for 35:55:10, 35:45:20, and 35:30:35 of

© 2011 WILEY-VCH Verlag GmbH & Co. KGaA, Weinheim

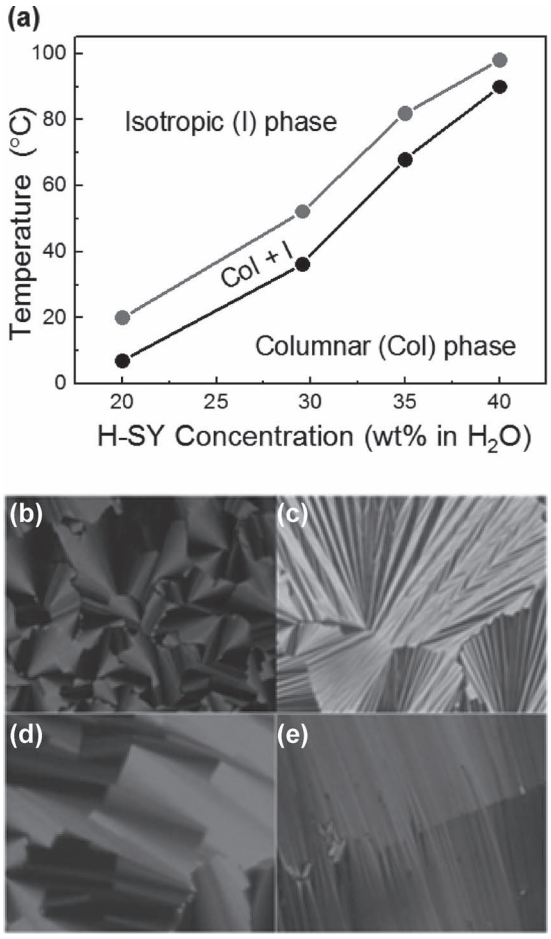

Figure 2. Phase diagram of a) H-SY/H_2O solution, and POM textures taken at room temperature of b) 25 wt%, c) 30 wt%, d) 35 wt%, and e) 40 wt% solutions, respectively.

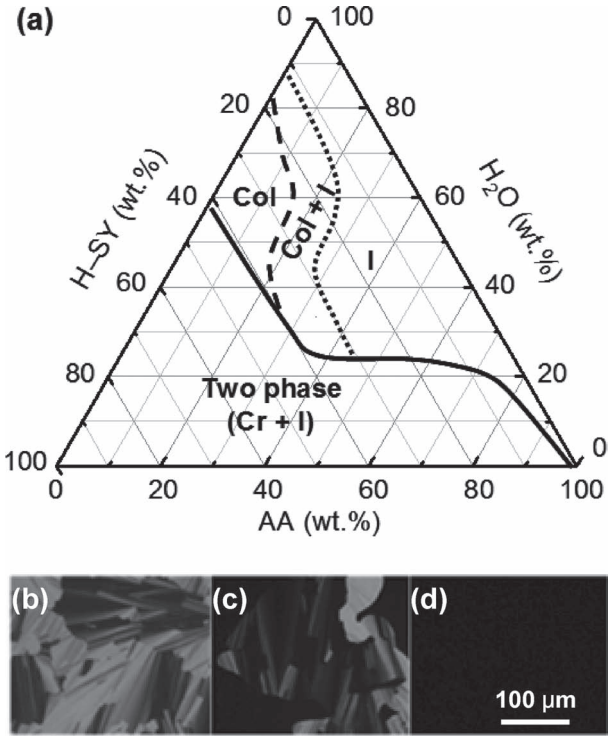

Figure 3. a) Ternary phase diagram of H-SY/H_2O/AA solution at 25 °C. POM textures of b) 35:55:10, c) 35:45:20, and d) 35:30:35 (H-SY:H_2O:AA by weight percentage) solutions, respectively.

H-SY/H_2O/AA by weight percentage, respectively. In Figure 3a, the region above the dotted line exhibits the I phase showing a complete dark-state under cross-polarized POM (Figure 3d). Similar to the case of H-SY/H_2O solution, H-SY/H_2O/AA solution forms a "biphase" of Col LC and I phase as the boundaries are designated by the dashed and dotted lines in Figure 3a POM image of the "biphase" is shown in Figure 3c. Further increasing the content of H-SY in H-SY/H_2O/AA solution results in the formation of the Col LC phase between the solid and the dashed lines (Figure 3a). The fan-shaped texture representing the Col LC phase is also shown in Figure 3b. Just below the solid line in Figure 3a, phase separation occurs and H-SY is precipitated as tiny crystalline aggregates out of the saturated H-SY/H_2O/AA solution.

Additionally, the existence of the Col LC phase in the H-SY/H_2O/AA solution between the solid and the dashed lines (Figure 3a) can be confirmed by the simple mechanical shearing using a doctor-blade coating method.[34,35] As shown in POM image (**Figure 4**a) which is prepared through doctor-blade coating, drying and subsequent UV-curing processes, it is obvious that H-SY aggregates are uniaxially oriented in a macroscopic length scale. This tentative conclusion can be validated by rotating the shear direction (SD) of the aligned H-SY film to be matched with the axis of polarizer or analyzer. POM image shown in Figure 4b exhibits a completely dark state when the SD of H-SY/PAA anisotropic film is parallel to the axis of polarizer. This means that H-SY molecules first self-assemble to columns in H-SY/H_2O/AA solution and the self-assembled H-SY columns are oriented along the SD during the doctor-blade coating. In addition, it is clear that molecular orientations and morphologies of the H-SY/PAA anisotropic films are successfully stabilized by the photo-polymerization of AA, which results in the uniformly aligned film without any macroscopic cracks. Note that the photo-polymerized poly(acrylic acid) (PAA) is an amorphous polymer so that PAA will not much contribute to the bi-refringence of POM images (Figures 4a and Figures 4b). Even though the polarized UV light can be employed to detect the molecular arrangements of the coatable anisotropic films,

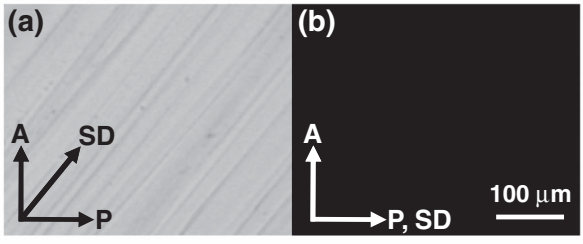

Figure 4. POM images of H-SY/PAA uniaxially oriented film (35 wt% solution): SD is a) 45° and b) parallel to the polarization axis. The A and P represent the direction of the trasmission axes of analyzer and polarizer, respectively, and SD stands for the shear direction of the anisotropic film.

© 2011 WILEY-VCH Verlag GmbH & Co. KGaA, Weinheim

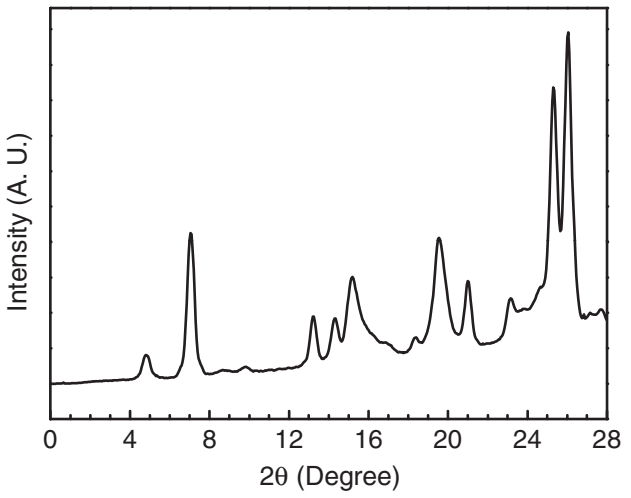

Figure 5. 1D WAXD pattern of H-SY/PAA powder prepared by grinding the H-SY films.

more detail molecular arrangements should be investigated by structure sensitive diffraction techniques.

2.2. Molecular Arrangement in the Anisotropically Oriented H-SY Film

In order to identify molecular arrangements in the oriented H-SY film, 1D WAXD experiment is first carried out and its 1D WAXD powder pattern is shown in **Figure 5**. H-SY powder sample is prepared by grinding the oriented H-SY film. In this 1D WAXD powder pattern, diffraction information about H-SY molecular arrangements appears on two different length scales. One is on the nanometer scale in the low 2θ-angle region between 1.5° and 11°, in which column packing information can be obtained. The other is on the sub-nanometer scale between 11° and 30°. Diffractions on the sub-nanometer scale can provide molecular packing information about the inside of columns as well as about molecular correlation between neighboring columns. As shown in Figure 5, four Bragg reflections at 2θ = 5.0, 5.2, 7.5, and 10.37° appear in the low 2θ-angle region which correspond to the d-spacings of 1.77, 1.70, 1.18, and 0.85 nm, respectively. On the basis of the triangulation method of building a 2D-a*b* lattice of the unit cell, these four Bragg reflections can be assigned to be the (100), (010), ($\bar{1}$10), and (020), respectively. However, this assignment is based on the assumption that these four reflections only come from the self-organization of columns. Through the refinement of the reciprocal 2D-a*b* lattice, a 2D unit cell in real space is calculated with the dimensions of a = 1.70 nm, b = 1.78 nm, and γ = 84.5°. Among many diffractions in the wide 2θ-angle region, the diffraction at 2θ = 26.3° (d-spacing = 0.34 nm) can be considered as a diffraction originated from the π-π interaction between H-SY molecules. Compared with 1D WAXD powder pattern of pristine H-SY, 1D WAXD powder pattern of H-SY/PAA is not distinguished, which means the photo-polymerized PAA does not much affect the crystalline structure of H-SY.

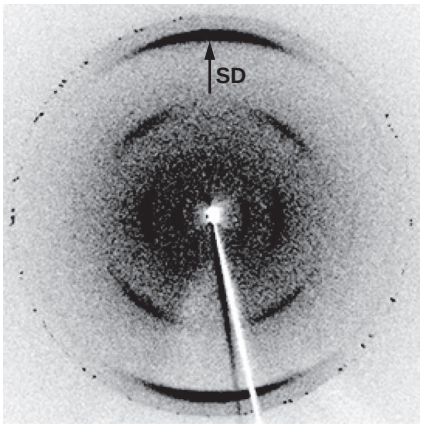

Figure 6. 2D WAXD pattern of H-SY/PAA anisotropic film fabricated by mechanical shearing of the 35 wt% H-SY/H_2O solution. Here, SD refers to the shear direction.

Even though 1D WAXD powder pattern of H-SY can provide all possible diffractions generated by H-SY crystalline structure, there are many limitations to identify the crystalline structure and molecular packings. Therefore, the information of 1D WAXD powder pattern should be combined with those of 2D WAXD and SAED of oriented films. As shown in **Figure 6**, 2D WAXD is obtained on an image plate by radiating X-ray normal to the oriented H-SY film. On the equator which is perpendicular to the shear direction (SD), only two diffractions are observed at 2θ = 5.2 (d-spacing = 1.70 nm) and 10.37° (d-spacing = 0.85 nm), which can be assigned as (010) and (020). This result is well matched with that of the 1D WAXD powder pattern (Figure 5). However, diffractions at 2θ = 5.0 and 7.5° are not observed in this 2D WAXD, which indicates that 2D WAXD obtained from the doctor-blade coated H-SY film is not a true fiber pattern. On the meridian of 2D WAXD, a pair of very strong diffraction arcs is observed at 2θ = 26.3°. As shown in Figure 6, this pair of diffraction arcs can be identified as the (002) plane. This assignment is supported by two pairs of diffused diffractions at 2θ = 17.3° (d-spacing = 0.516 nm) in four quadrants. Therefore, it can be considered that the (001) diffraction at 2θ = 13.15° on the meridian is extinct. This result and analysis indicate that H-SY molecules are self-assembled into columns with a fashion of AB stacking and that the plane normal direction of H-SY aromatic core is parallel to the long axis of the assembled columns. The AB stacking should be generated to minimize the steric hindrance and electrostatic repulsion between neighboring sulfuric acids and to maximize the π–π interaction between H-SY aromatic cores. Two pairs of diffused diffractions in four quadrants (2θ = 17.3°) can be explained by three possible reasons. One is that the stacked H-SY molecules inside of the columns are tilted ±51.4° with respect to the long axis of columns, which leads to the diffraction located at ±38.6° out of the meridians. Another is that the H-SY molecule is not on the same plane but forms a bent conformation with an angle of 29.5°. The final possible reason can be found from the H-SY molecular packing correlations between columns. This means that H-SY molecule retains the most stable flat conformation and the flat H-SY discs are AB-stacked without tilting with respect to the long axis of columns. In this situation, two pairs of diffused diffractions in

© 2011 WILEY-VCH Verlag GmbH & Co. KGaA, Weinheim

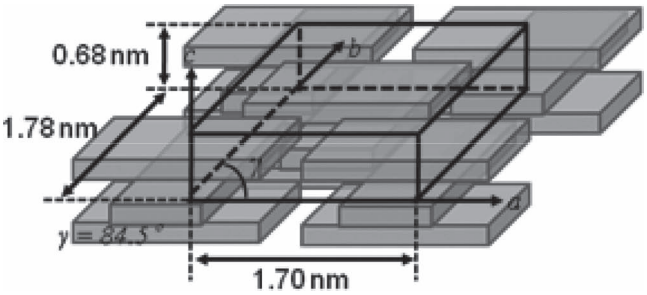

Figure 7. Schematic diagrams of the self-assembled H-SY crystalline phase.

four quadrants are originated from the crystallographic planes generated by the H-SY molecular packing correlations between columns. However, in order to find the most probable reason for these diffractions at $2\theta = 17.3°$, these hypotheses should be tested out by utilizing polarized spectroscopes, which will be discussed later in this paper. The crystallite size of H-SY film along the long axis of column is ~20 nm, which is estimated by Scherrer's equation.[8,9] The H-SY column length in H-SY/PAA film is also evaluated to be ~4.7 nm which is lower than that of the pristine H-SY film. This means that PAA or AA more or less hinder the self-assembly of H-SY into columns even though they do not change the crystalline structure of H-SY. From the combined results of 1D and 2D WAXD and careful structural analysis, the structure of H-SY is identified as a monoclinic crystal with unit cell dimensions of a = 1.70 nm, b = 1.78 nm, c = 0.68 nm, $\alpha = \beta = 90$ ° and $\gamma = 84.5$ ° via the refinement of the reciprocal lattice. This phase can thus be identified as a columnar crystalline (K_M) phase. The molecular arrangement inside of the monoclinic unit cell of K_M phase is also proposed based on the 2D WAXD result (**Figure 7**). The experimentally observed and the calculated 2θ values and d-spacings based on this unit cell lattice are listed in **Table 1**. Its calculated crystallographic density is 1.40 g cm^{-3} based on four H-SY molecules per unit cell which is well agreed with the experimentally measured density (1.40 g cm^{-3}).[36]

This structure determination can also be supported by TEM morphology and SAED pattern experiments, as shown in **Figure 8**. From the bright-field TEM images of the pristine H-SY (Figure 8a) and H-SY/PAA (Figure 8b) films, it is very obvious that the pristine H-SY film contains a lot of macroscopic cracks along the SD, while the H-SY/PAA film exhibits a smooth surface. The cracks in the pristine H-SY film are generated because of the anisotropic volume shrinkage during crystallization and H_2O evaporation. SAEDs of the pristine H-SY (Figure 8c) and H-SY/PAA (Figure 8d) films are very similar to 2D WAXDs but high ordered diffractions are additionally observed in SAEDs. From the (002) diffractions on the meridian, it is confirmed that molecular orientations and correlation length of columns in the pristine H-SY film are higher than those of the H-SY/PAA film, which agrees well with the result of 2D WAXD. This indicates that H-SY crystals in the H-SY/PAA film are in a metastable state compared with those in the pristine H-SY film. Comparing SAED of the pristine H-SY film with that of the H-SY/PAA film, it can be seen that the d-spacings and symmetries of SAED patterns are equivalent to each other. This result again indicates that the AA monomer and its polymerized PAA polymer do not affect the H-SY molecular packings even though the degree of orientation and crystallite size can be changed. However, it is worthwhile nothing that on SAED of the H-SY/PAA film, there is a pair of amorphous halos on the equator at the d-spacing = 0.24 nm, which is not observed

Table 1. Experimental and calculated crystallographic parameters of the monoclinic crystalline structure (K_M) of H-SY.

	2θ [deg]		d-spacing [nm]	
hkl	expt[a)]	calc[b)]	expt[a)]	calc[b)]
100	5.0	4.99	1.77	1.77
010	5.2	5.22	1.70	1.69
$\bar{1}10$	7.5	7.56	1.18	1.17
020	10.37	10.45	0.85	0.85
011	14.10	14.04	0.63	0.63
$\bar{2}20$	15.27	15.15	0.58	0.58
$\bar{3}10$	16.21	16.36	0.55	0.54
201	17.30	16.63	0.52	0.53
230	17.95	17.81	0.49	0.50
$\bar{2}30$	19.65	19.45	0.45	0.46
240	22.65	22.40	0.39	0.40
$4\bar{1}1$	22.57	22.40	0.36	0.37
002	26.37	26.21	0.33	0.34
$\bar{1}12$	27.35	27.32	0.32	0.32

[a)]The accuracy of the experimental data is ± 0.005 nm; [b)]The calculated data listed are based on the monoclinic crystalline (K_M) unit cell with a = 1.70 nm, b = 1.78 nm, c = 0.68 nm, $\alpha = \beta = 90.0°$ and $\gamma = 84.5°$.

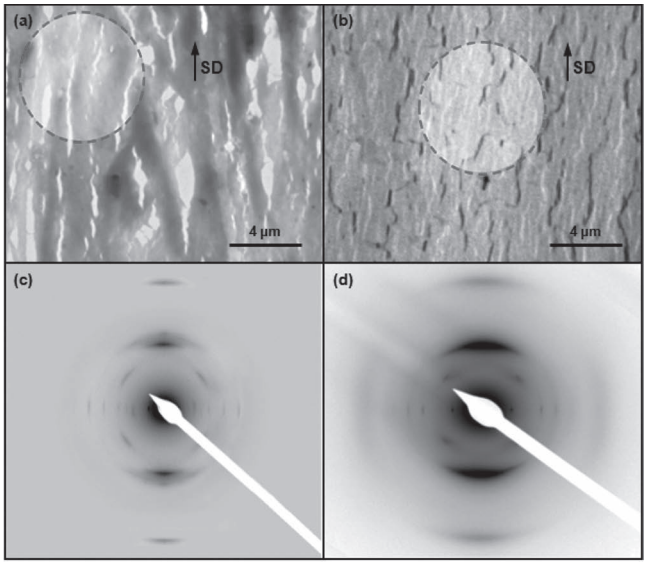

Figure 8. Bright-field TEM images of the aligned H-SY films coated with a) the 35 wt% H-SY/H_2O and b) the 35:30:35 (H-SY:H_2O:AA by weight ratio) solutions, respectively. c–d) SAED patterns from circled areas of Figure 8a (c) and Figure 8b (d).

© 2011 WILEY-VCH Verlag GmbH & Co. KGaA, Weinheim

on the pristine H-SY film. This pair of amorphous halos originating from the inter-molecular distance of PAA indicates that PAA polymers are partially aligned parallel to the SD. From the SAED experiments combined with the 2D WAXD results, it is concluded that H-SY crystals are embedded in the PAA matrix and H-SY molecules do not make one-to-one interactions with carboxylic acid moeities of PAA during crystallization.

2.3. Molecular Interactions and Polarizability of the Uniaxially Oriented H-SY/PAA Films

FT IR spectroscopy is useful for investigating the intra-/inter-molecular interactions with neighboring molecules and for examining the molecular orientations when the incident light is polarized.[37–41] By varying polarization axis from 0 to 90° with respect to the SD, polarized FT IR spectra of H-SY anisotropic films fabricated from 35 wt% H-SY/H_2O and 7:6:7 (H-SY:H_2O:AA at weight ratio) solutions are obtained and represented in **Figure 9**a, c, e, and Figure 9b, d, f, respectively. The vibrational modes of H-SY molecule are assigned as shown in Figure 9a, c, e, and their results are well matched with those reported in the literature.[42–44] The naphthalene stretching vibrations are found to make a major contribution with intense absorption bands at wavenumbers in the range of 1640 and 1400 cm^{-1}, in which a very strong absorption band at 1506 cm^{-1} (Figure 9a) is a consequence of the coupling effect of naphthalene ring and asymmetric azo stretching vibrations.[44] Note that azo stretching vibrations partially contribute the absorption bands between 1350 and 1200 cm^{-1} and overlap with those of naphthalene vibrations. Additionally, the absorption bands at 1120, 1096, and 1004 cm^{-1} are mainly contributed by the bending vibrations of naphthalene ring, and the out-of-plane bending vibrations of naphthalene ring are observed at wavenumbers between 1000 and 675 cm^{-1}.[46] Strong absorption bands in the range of 1180–1209 cm^{-1} wavenumbers stand for the SO_3 stretching vibrations. The absorption bands at 1167 and 1032 cm^{-1} can be identified as the SO_3 asymmetric and symmetric stretching vibrations, respectively. Additionally, the SO_3 symmetric deformation vibrational band is found at 667 cm^{-1}.[47,48]

H-SY molecular orientation in the uniaxially coated H-SY film can be evaluated by polarized FT IR. As rotating the axis of polarizer with respect to the SD from 0° to 90°, polarized FT IR spectra of H-SY anisotropic films are obtained, as shown in Figure 9a, c and e. By increasing the azimuthal angle from 0° (parallel to the shear direction) to 90° (perpendicular to the SD), the strong absorption band at 1167 cm^{-1} due to the SO_3 asymmetric stretching vibration is continually decreased while the rest of vibrations including naphthalene and azo vibrations show the maximum absorption when the SD is parallel to the polarizer (azimuthal angle = 0°). Based on the polarized FT IR data combined with the 2D WAXD results, it is concluded that the aromatic moieties, C–N bond and C–H bond are on the same plane and that the in-plane axis of H-SY discotic core is perpendicular to the SD while the long axis of S=O group is parallel to the SD. Therefore, it is concluded that H-SY are self-assembled into columns and the long axis of columns are parallel to the SD.

As shown in Figure 9b, d and f, polarized FT IR spectra of H-SY/PAA anisotropic films are also measured by rotating the axis of polarizer with respect to the SD from 0° to 90°. From these FT IR spectra, it is immediately recognized that there is one more absorption band with a maximum intensity at 1720 cm^{-1} and the rest of absorption bands are identical to those of the pristine H-SY anisotropic films. The absorption band at 1720 cm^{-1} can be identified as the stretching vibrational band of carbonyl bond and this band does not depend on the azimuthal angles, as shown in Figure 9b. This result again confirms that H-SY crystals are embedded in the amorphous PAA matrix and H-SY molecules do not form one-to-one interactions with carboxylic acid functions of PAA during crystallization, which agrees well with the results of 2D WAXD (Figure 6) and SAED (Figure 8d).

Although the molecular orientations in the H-SY and H-SY/PAA films are investigated by 2D WAXD, SAED, and polarized FT-IR, the polarizability of the H-SY and H-SY/PAA anisotropic films in visible regions should be evaluated by polarized UV–vis spectroscopy. Polarized UV–vis spectra of the H-SY film are obtained in a transmission mode,[49] as shown in **Figure 10**a. When the polarization axis of incident light is perpendicular to the SD (azimuthal angle = 90°), the H-SY film absorbs light to its maximum while a weak absorption occurs when the polarization axis of the incident light is parallel to the SD (azimuthal angle = 0°).[50] This result corroborates that H-SY molecules self-assemble to columns and the long axis of columns are parallel to SD so that a polarized light perpendicular to the SD is absorbed most by H-SY molecules.[36,37] Degree of polarization (DOP), defined as DOP = $(T_0 - T_{90})/(T_0 + T_{90})$,[17,19] of the H-SY film can be obtained from the UV–vis spectra shown in Figure 10a. Here, T_0 and T_{90} represent the transmittances when the azimuthal angles are 0° and 90°, respectively. Since DOP is a function of film thickness, DOP should be normalized with respect to the transmittance of light. As shown in Figure 10b, the normalized DOP spectra can be obtained and directly compared with DOP of other polarizers when the mean transmittance ($T_{Single} = (T_0 + T_{90})/2$) is normalized to be 40% at the maximum absorption wavelength (λ_{max} = 473 nm). DOP of the H-SY/PAA film is also evaluated and presented in Figures 10c and Figures 10d. DOPs (T_{Single} = 40%) of the H-SY and H-SY/PAA films at λ_{max} = 473 nm are 98% and 80%, respectively. The lower DOP of the H-SY/PAA film compared with that of the H-SY anisotropic film could arise from the fact that the H-SY molecular orientation becomes lower during the photo-polymerization of AA. This explanation coincides with the results of SAED and polarized FT-IR. The lower DOP of the H-SY/PAA film is believed to be improved by the optimized processes of coating, crystallization and polymerization. Furthermore, from the DOP spectrum shown in Figure 10b, it is realized that in order to polarize the whole visible region, other LCLCs which can cover the polarization between 500 and 700 nm should be applied together. One of methods to fabricate a LCLC-based polarizer covering the whole visible region is to fabricate multi-layers with different LCLCs, in which mechanical and chemical stabilities of each LCLC layer should be assured.

2.4. Stabilization of H-SY/PAA Anisotropic Film and Fabrication of Patterned Polarizer

Mechanical stability of the aligned H-SY/PAA film is estimated by the pencil hardness test (ASTM D3363–00) and

© 2011 WILEY-VCH Verlag GmbH & Co. KGaA, Weinheim

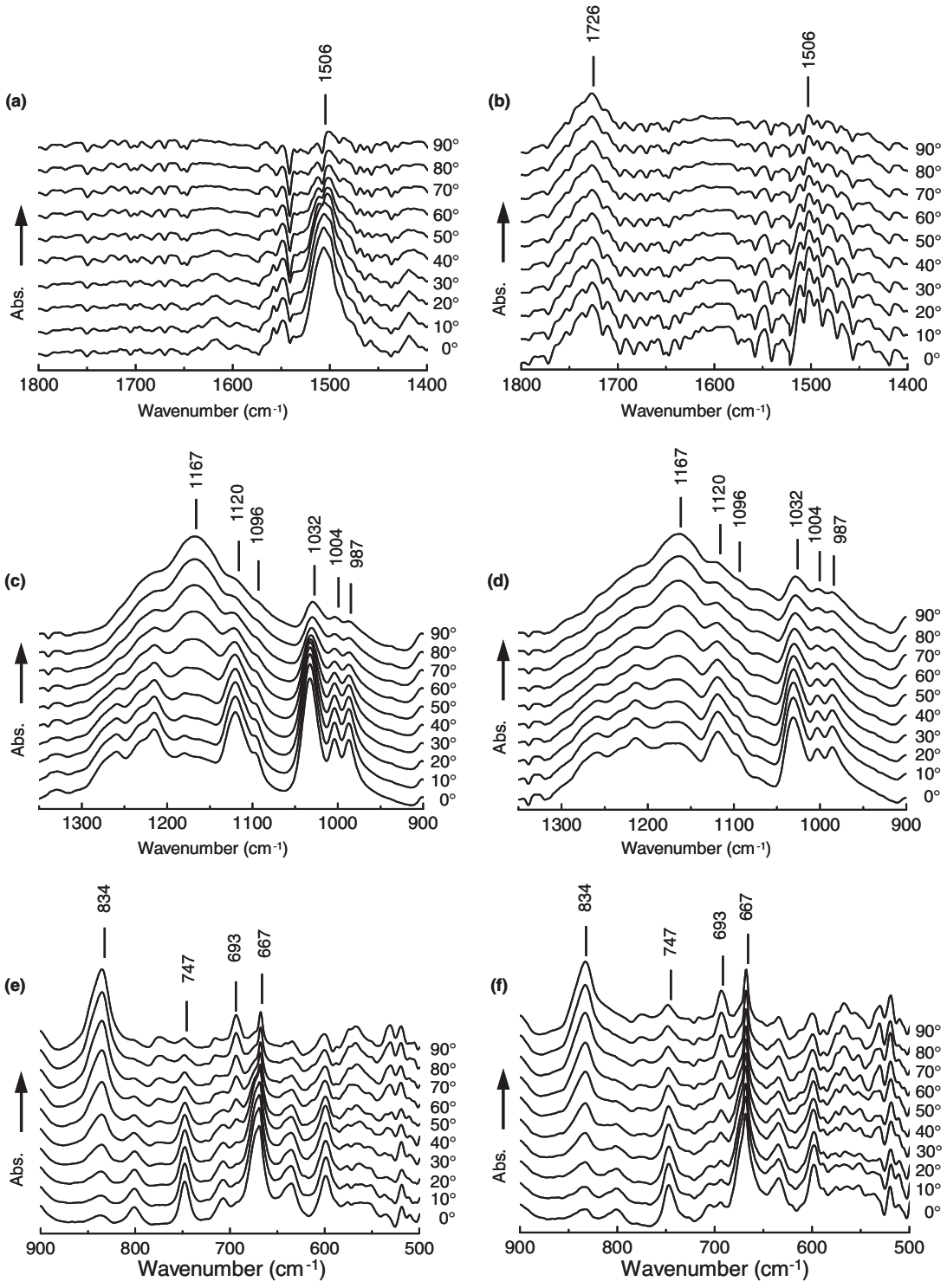

Figure 9. a,c,e) Polarized FT IR spectra for the aligned H-SY films fabricated from the 35 wt% H-SY/H_2O and b,d,f) the 35:30:35 (H-SY:H_2O:AA by weight ratio) solutions by rotating the polarization axis from 0 to 90°.

its result is compared with that of the pristine H-SY film, as shown in **Figure 11**a–j. By increasing the pencil hardness from 5B (Figure 11a, f), F (Figure 11b, g), HB (Figure 11c, h), 2H (Figure 11d, i) to 4H (Figure 11e, j), the pristine H-SY film starts to be scratched above F while the H-SY/PAA anisotropic film resists against the pencil scratching up to H. This result clearly demonstrates that the mechanical stability of H-SY/PAA anisotropic film is significantly improved by the photo-polymerization of AA.

© 2011 WILEY-VCH Verlag GmbH & Co. KGaA, Weinheim

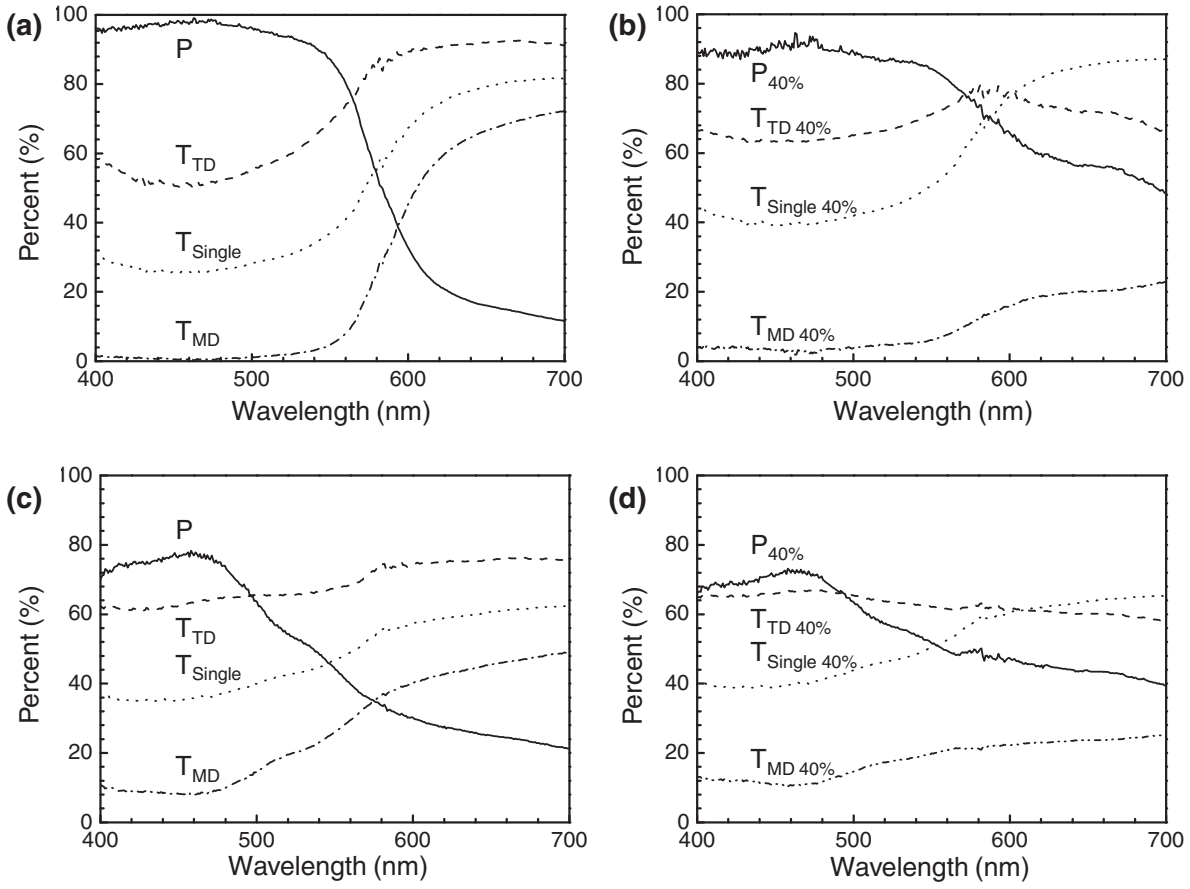

Figure 10. a–b) UV–vis spectra for the aligned H-SY films from the 35 wt% H-SY/H_2O and c–d) the 35:30:35 (H-SY:H_2O:AA by weight ratio) solutions. Figure 10a and 10c, and Figure 10b and 10d are the degree-of-polarization (DOP) as a function of wavelength before and after the 40% normalization of transmittance, respectively.

Chemical stability of the pristine H-SY and H-SY/PAA films is also tested by dropping various solvents on the films and the results are tabulated in **Table 2**. Even though molecular orientations and morphologies of the pristine H-SY and H-SY/PAA films are damaged by the attack of aqueous solvents with strong base (NaOH) and acid (HCl), the H-SY/PAA anisotropic films can withstand in common organic solvents. Based on the mechanical and chemical stability tests, it is concluded that the photo-polymerization of AA is a robust method to protect the LCLC-based anisotropic films. Furthermore, it is worth noting that by introducing AA and subsequent photo-polymerization, it is possible to fabricate the in-cell polarizer on the flexible

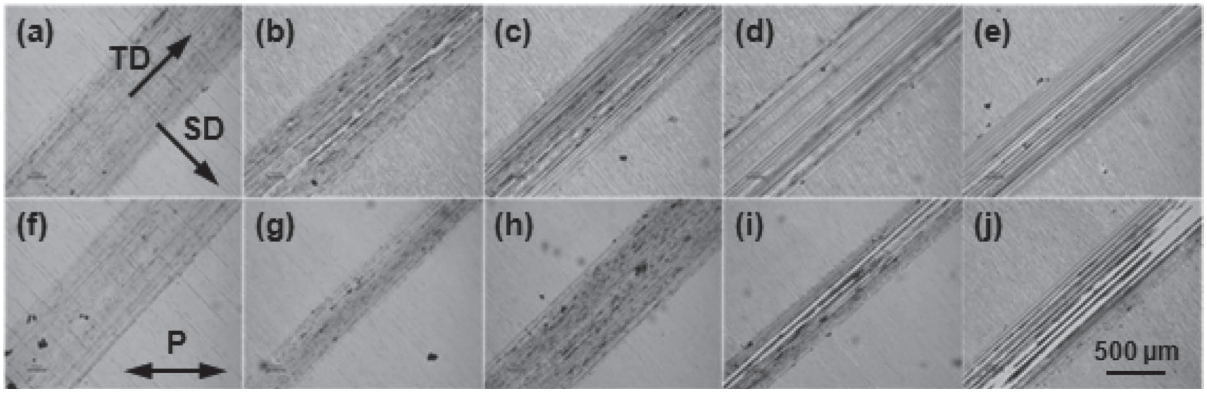

Figure 11. POM images after the pencil hardness test of the pristine H-SY (a–e) and the H-SY/PAA anisotropic (f–j) films. Pencils were used with different hardnesses: 5B, (a, f), F (b, g), HB (c, h), 2H (d, i), and 4H (e, j). TD and SD refer to the test direction for pencil hardness and the shear direction, respectively.

© 2011 WILEY-VCH Verlag GmbH & Co. KGaA, Weinheim

Table 2. Chemical stabilities of the H-SY and H-SY/PAA films

	H-SY	H-SY/PAA
0.1N HCl	X	X
0.1N NaOH	X	X
H_2O	X	X
EtOH	X	○
Acetone	□	○
IPA	X	○
Hexane	□	○
Toluene	□	○
EA	X	□
MC	X	□
PET ether	□	□
THF	X	□

○: stable, □: partial wash, X: perfect wash, isopropyl alcohol (IPA), ethyl acetate (EA), methylene chloride (MC), petroleum ether (PET ether), and tetrahydrofuran (THF).

polymer substrate which is one of the key components for flexible displays.

It may be possible to fabricate a patterned H-SY/PAA polarizer if a photo-mask is applied during the UV photo-polymerization. In order to realize this proposal, the photo-mask with 1D striped pattern is arranged parallel to the SD of the H-SY/AA films and AA monomers are selectively photo-polymerized, and then the unpolymerized part is washed away with ethyl acetate (EA) solvent. POM images of the patterned H-SY/PAA polarizer are shown in **Figure 12**a and Figure 12b when the SD is 45° and parallel to polarizer, respectively. Here, the intensity of incident light is increased to obtain clear POM images. It is obvious that the uniaxial orientation of H-SY molecule in the LC phase is retained during the photo-polymerization and the developing processes. Patterned polarizers fabricated by a simple coating and photo-polymerization may pave new pathways for the applications of LCLC to electro-optic devices, especially for the optical devices requiring polarized light in a local area.[51–53]

3. Conclusions

The anisotropic LCLC film, which is certain to be a component for flexible displays, was successfully fabricated from H-SY. H-SY-based uniaxial LCLC film was further stabilized via the photo-polymerization of AA monomer. Molecular packing structures and optical behaviors of the anisotropically oriented H-SY films were investigated by the combined techniques of microscopy, scattering, and spectroscopy. Phase behaviors of H-SY/H_2O/AA solution were monitored by varying compositions of the solution by using POM. Based on the experimental results obtained by 2D WAXD combined with those of SAED, H-SY crystalline unit cell was determined to be monoclinic with the dimensions of a = 1.70 nm, b = 1.78 nm, c = 0.68 nm, $\alpha = \beta$ = 90.0° and γ = 84.5°, and its molecular packing model was also proposed. It was realized that the photo-polymerization of AA in H-SY/H_2O/AA solution did not change the structural dimensions. The molecular arrangements in the oriented H-SY films were further confirmed by polarized FT-IR and polarized UV–vis spectroscopies. The scratch resistance evaluated through the pencil hardness test represented that the mechanical stability was significantly enhanced after the photo-polymerization. Chemical stabilities of the pristine H-SY and H-SY/PAA films were also tested by dropping various solvents on the films. Based on the mechanical and chemical stability tests, it was concluded that the photo-polymerization of AA is a robust method to protect the LCLC-based anisotropic films. Utilizing polarized UV–vis spectrometer, the DOP of the oriented H-SY films with and without the photo-polymerization was also evaluated to be 80% and 98%, respectively. Additionally, patterned polarizers fabricated by a simple lithographic method may provide more opportunities for novel applications of LCLC to electro-optic devices.

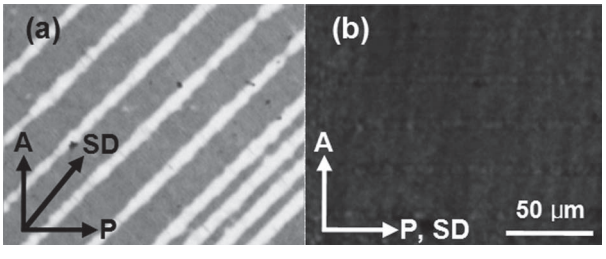

Figure 12. POM images of the patterned H-SY/PAA anisotropic film: a) SD is 45° and b) parallel to the polarization axis. Here, A and P indicate the direction of the optical axis of the polarizer, and SD refers to the shear direction of the film.

4. Experimental Section

Materials and Sample Preparation: Sunset Yellow FCF (abbreviated as SY-FCF, 95.7% purity) purchased from Sigma Aldrich was purified several times by washing with ethanol and deionized water. The purity of SY-FCF was estimated to be over 99.0% according to the HPLC test. Due to the existence of Na^+ ions in SY-FCF, unexpected side effects may occur in applying it as an optical material. Therefore, the Na^+ ions in SY-FCF were substituted to the H^+ ions by proton exchange reaction for 2 h. Dowex G-26 (H-form, Dow Chemicals), a polystyrene-based strongly acidic cation exchanger, was used for the proton exchange process. For the proton exchange process, H-form Dowex G-26 was first washed with an aqueous HCl solution to remove organic and inorganic impurities and then with distilled water. The completion of the proton exchange reaction was confirmed by pH and Fourier transform infrared (FT-IR) measurements. The pH of H-SY was 1.88, which was estimated by pH-meter (JEIO Tech. Nr.04310034). The chemical structure of H-SY is shown in Figure 1a. The molecular weight of H-SY is 408.0 g mol^{-1}. The H-SY anisotropic films were stabilized by the photo-polymerization of acrylic acid (AA, Sigma Aldrich). Here, AA works not only for a monomer but also for a solvent. AA was purified by the copper gauze packed column distillation to remove inhibitors, such as methylene blue.

According to the degree of molecular orientations estimated by cross-polarized optical microscopy (POM) and polarized ultraviolet–visible (UV–vis) spectroscopies, the compositions of H-SY/H_2O (35 wt% H-SY in 65 wt% deionized H_2O) and H-SY/H_2O/AA (1:1:1 in weight ratio) solutions were optimized.[54,55] The anisotropic films were prepared by the doctor blade-coating of H-SY/H_2O or H-SY/H_2O/AA solution on bare glasses and the subsequent drying at room temperature for 24 h to eliminate water. The thicknesses of films were controlled to be 1–100 μm by changing the height of doctor-blade. Additionally, when H-SY/H_2O/AA solution was used, AA was photo-polymerized by exposing UV light with wavelengths in the range of 200–2500 nm for 15 min right after the

© 2011 WILEY-VCH Verlag GmbH & Co. KGaA, Weinheim

drying process. To construct phase diagrams using POM observations, the original concentrations were kept constant by sealing the edge of sandwiched LC cells with epoxy resin.

For the one-dimensional (1D) wide angle X-ray diffraction (WAXD) measurements, isotropic powder samples obtained by grinding anisotropic films were mounted on the amorphous polyimide tape.[56] To obtain structure information utilizing 2D WAXD and POM, uniaxially coated films with 10 μm thickness were used. Density measurements were carried out at room temperature using a Guy-Lussac type specific gravity bottle (10 mL) which was calibrated using the ASTM D 369 method. The experimentally observed density values were used to judge the number of molecules in the crystalline unit cells. The anisotropic films prepared for polarized Fourier transform infrared (FT-IR) spectroscopy and polarized ultraviolet-visible (UV–vis) spectroscopies were prepared with a thickness in the range of 1–10 μm. For transmission electron microscopy (TEM), anisotropic films with a thickness of 150–300 nm were coated on carbon-coated mica. After the photo-polymerization process, the films were floated onto the water surface and recovered using the TEM copper grids.

The scratch resistance of the coatable anisotropic films was evaluated by the pencil hardness test using the STAEDTLER Mars Lumograph 100-G12.[57] Additionally, the chemical stability of coatable anisotropic films was estimated based on the POM images of specimen after dropping various solvents on the surface of coatable anisotropic films. Furthermore, for the fabrication of micrometer-scale patterned anisotropic films, the area-selective photo-polymerization of AA was performed by exposing UV lights through a photomask.[58]

Equipment and Experiments: Optical textures were observed with a POM (Nikon Dxm 1200) coupled with a Linkam heat stage (TMS94) to investigate morphology on the micrometer scale, to construct the phase diagrams of the H-SY/H_2O and H-SY/H_2O/AA solutions and to evaluate the chemical and mechanical stabilities of the uniaxially aligned films.

1D WAXD experiments were carried out in the reflection mode of a Rigaku 12 kW rotating-anode X-ray (Cu Kα radiation, wavelength = 0.154 nm) generator coupled to a diffractometer. The position and width of diffraction peaks were calibrated with silicon crystals of known crystal size in the high 2θ-angle region (> 15°) and silver behenate in the low 2θ-angle region. Samples were scanned across a 2θ-angle range of 1.5 to 30° at a scanning rate of 2.5 ° min^{-1}.

In order to obtain the unit cell dimension and symmetry of crystal, 2D WAXD experiments on the oriented samples were conducted using an imaging system (Rigaku, R-AXIS-IV) with an 18 kW rotating anode X-ray generator. Silicon crystal powder, used as an internal reference, shows a diffraction ring at a 2θ value of 28.466°. A 30 min exposure time was required for a high-quality pattern. In both 1D and 2D WAXD experiments, background scatterings were subtracted from the sample scans.

Bright-field images of TEM (FEI Tacnai 12) were obtained to examine crystal morphology on a nanometer scale using an accelerating voltage of 120 kV. The identified molecular packing structures by 2D WAXD were confirmed by selected area electron diffraction (SAED). The camera length was set at 2.0 m and calibration of SAED spacing smaller than 0.384 nm was carried out using evaporated thallous chloride, which has the largest first-order diffraction at d = 0.384 nm. The d-spacing values larger than 0.384 nm were estimated by doubling the d-spacing values of the first-order diffractions.

Molecular interactions and degree-of-polarization (DOP) in the uniaxially oriented films were evaluated by polarized FT IR (Jasco FT/IR-300E)[59,60] and polarized UV–vis (Scinco S-3100) spectroscopies by rotating the polarizer transmission axis from 0° to 90° with respect to the SD of the films. The resolutions of FT IR and UV–vis spectra were 1 cm^{-1} and 0.5 nm, respectively, and 40 scans were averaged for each spectrum. Polarized FT IR was also applied to identify the orientation of H-SY molecules with respect to the long axis of the LCLC column. DOP and single transmittance (T_{Single}) of the anisotropic films can be calculated from the polarized UV–vis transmittance spectra of the H-SY/H_2O and H-SY/H_2O/AA films.[61,62] Additionally, the Cerius^2 (Version 4.6) simulation software from Accelrys was also used to calculate the minimal energy geometry of the H-SY in the isolated gas-phase utilizing the COMPASS force field.

Acknowledgements

This work was mainly supported by Fundamental R&D Program for Core Technology of Materials (MKE) and NRF-2010–0007562, Korea. S.W.K and S.H.L are also grateful for the support from WCU-R31–20029 (MEST, Korea). Note: This article was amended on June 7, 2011 to correct the nomenclature in Figure 2 and 3, which was incorrect in the version originally published online.

Received: December 2, 2010
Revised: February 22, 2011
Published online: April 20, 2011

[1] J. Lyndon, in *Handbook of Liquid Crystals*, Vol. *2B* (Eds: D. Demus, J. Goodby, G.W. Gray, H.-W. Spiess, V. Vill), Wiley-VCH: Weinheim, Germany **1998**, pp. 981.
[2] J. Lydon, *J. Mater. Chem.* **2010**, *20*, 10071.
[3] D. L. Gin, X. Lu, P. R. Nemade, C. S. Pecinovsky, Y. Xu, M. Zhou, *Adv. Funct. Mater.* **2006**, *16*, 865.
[4] S.-W. Tam-Chang, W. Seo, K. Rove, S. M. Casey, *Chem. Mater.* **2004**, *16*, 1832.
[5] L. Wang, K.-U. Jeong, M.-H. Lee, *J. Mater. Chem.* **2008**, *18*, 2657.
[6] S. W. Kang, Q. Li, B. D. Chapman, R. Pindak, J. O. Cross, L. Li, M. Nakata, S. Kumar, *Chem. Mater.* **2007**, *19*, 15657.
[7] S. V. Shiyanovskii, O. D. Lavrentovich, T. Schneider, T. Ishikawa, I. I. Smalyukh, C. J. Woolverton, G. D. Niehaus, K. J. Doane, *Mol. Cryst. Liq. Cryst.* **2005**, *434*, 587.
[8] K.-U. Jeong, A. J. Jing, B. Monsdorf, M. J. Graham, F. W. Harris, S. Z. D. Cheng, *J. Phys. Chem. B* **2007**, *111*, 767.
[9] S.-J. Park, S.-H. Hwang, N. Kim, S.-W. Kuo, H. Y. Kim, S.-K. Park, Y.-J. Kim, C. Nah, J. H. Lee, K.-U. Jeong, *J. Phys. Chem. B* **2009**, *113*, 13499.
[10] H. P. Rathnayake, A. Cirpan, Z. Delen, P. M. Lahti, F. E. Karasz, *Adv. Funct. Mater.* **2007**, *17*, 115.
[11] C. B. McKitterick, N. L. Erb-Satullo, N. D. LaRacuente, A. J. Dickinson, P. J. Collings, *J Phys. Chem. B* **2010**, *114*, 1888.
[12] S.-W. Tam-Chang, I. K. Iverson, K. Helbley, *Langmuir* **2004**, *20*, 342.
[13] N. H. Hartshorne, G. D. Woodward, *Mol. Cryst. Liq. Cryst.* **1993**, *23*, 343.
[14] D. Goldfard, Z. Luz, N. Spielberg, Zimmermann, *Mol. Cryst. Liq. Cryst.* **1985**, *126*, 225.
[15] H.-S. Park, S.-W. Kang, L. Tortora, Y. Nastishin, D. Finotello, S. Kumar, O. D. Lavrentovich, *J. Phys. Chem. B* **2008**, *112*, 16307.
[16] S. V. Shiyanovskii, T. Schneider, I. I. Smalyukh, T. Ishikawa, G. D. Niehaus, K. J. Doane, C. J. Woolverton, O. D. Lavrentovich, *Phys. Rev. E* **2005**, *71*, 020702.
[17] H. R. Stapert, S. Valle, E. J. K. Verstegen, D. M. I. Zande, J. Lub, S. Stallinga, *Adv. Funct. Mater.* **2003**, *13*, 732.
[18] S.-W. Tam-Chang, W. Seo, I. K. Iverson, S. M. Casey, *Angew. Chem., Int. Ed.* **2003**, *42*, 897.
[19] C. D. West, R. C. Jones, *J. Opt. Soc. Am.* **1951**, *41*, 976.
[20] E. Charlet, E. Grelet, P. Brettes, H. Bock, H. Saadaoui, L. Cisse, P. Destruel, N. Gherardi, I. Seguy, *Appl. Phys. Lett.* **2008**, *92*, 024107.
[21] T. Schneider, K. Artyushkova, J. E. Fulghum, L. Broadwater, A. Smith, O. D. Lavrentovich, *Langmuir* **2005**, *21*, 2300.
[22] T. Schneider, O. D. Lavrentovich, *Langmuir* **2000**, *16*, 5227.
[23] K. V. Kaznatcheev, P. Dudin, O. D. Lavrentovich, A. P. Hitchcock, *Phys. Rev. E* **2007**, *76*, 061703.
[24] K. Mundy, J. C. Sleep, J. E. Lydon, *Liq. Cryst.* **2005**, *19*, 107.
[25] T. Sergan, T. Schneider, J. Kelly, O. D. Lavrentovich, *Liq. Cryst.* **2000**, *27*, 567.
[26] B. Chae, S. B. Kim, S. W. Lee, S. I. Kim, W. Choi, B. Lee, M. Ree, K. H. Lee, J. C. Jung, *Macromolecules* **2002**, *35*, 10119.

© 2011 WILEY-VCH Verlag GmbH & Co. KGaA, Weinheim

[27] Y.-W. Lim, C.-H. Kwak, S.-D. Lee, *J. Nanosci. Nanotechnol.* **2008**, *8*, 4775.
[28] Y.-W. Lim, D.-W. Kim, S.-D. Lee, *Mol. Cryst. Liquid Cryst*. **2008**, *489*, 183.
[29] J. J. Ge, C. Y. Li, G. Xue, I. K. Mann, D. Zhang, S.-Y. Wang, F. W. Harris, S. Z. D. Cheng, S.-C. Hong, X. Zhuang, Y. R. Shen, *J. Am. Chem. Soc.* **2001**, *123*, 5768.
[30] H. Chang, G. Wang, A. Yang, X. Tao, X. Liu, Y. Shen, Z. Zheng, *Adv. Funct. Mater.* **2010**, *20*, 2893.
[31] J. E. Lydon, *Curr. Opin. Colloid Interface Sci.* **2004**, *8*, 480.
[32] C. Nuckolls, R. Shao, W.-G. Jang, N. A. Clark, D. M. Walba, T. J. Katz, *Chem. Mater.* **2002**, *14*, 773.
[33] D. J. Edwards, J. W. Jones, O. Lozman, A. P. Ormerod, M. Sintyureva, G. J. T. Tiddy, *J. Phys. Chem. B* **2008**, *112*, 14628.
[34] J. Q. Carou, N. J. Mottram, S. K. Wilson, B. R. Duffy, *Liq. Cryst* **2007**, *34*, 621.
[35] M. I. Bodnarchuk, M. V. Kovalenko, S. Pichler, G. Fritz-Popovski, G. Hesser, W. Heiss, *ACS Nano* **2010**, *4*, 423.
[36] R. J. Luoma, Ph.D. dissertation, Brandeis University, **1995**.
[37] F. Ambrosino, S. Califano, *Spectrochim. Acta* **1965**, *21*, 1401.
[38] P.-A. Chollet, J. Messier, C. Rosilio, *J. Chem. Phys.* **1976**, *64*, 1042.
[39] M. Tammer, J. J. Li, A. Komp, H. Finkelmann, F. Kremer, *Macromol. Chem. Phys.* **2005**, *206*, 709.
[40] S. V. Shilov, S. Okretic, H. W. Siesler, M. A. Czarnecki, *Appl. Spectrosc. Rev.* **1996**, *31*, 125.
[41] H. Skupin, F. Kremer, S. V. Shilov, P. Stein, H. Finkelmann, *Macromolecules* **1999**, *32*, 3746.
[42] M. Snehalatha, N. Sekar, V. S. Jayakumar, I. H. Joe, *Spectrochim. Acta Part A* **2008**, *69*, 82.
[43] K. H. Kim, K. Ishikawa, H. Takezoe, A. Fukuda, *Phys. Rev. E* **1995**, *51*, 2166.
[44] M. Snehalatha, C. Ravikumar, I. H. Joe, *Solid State Sci.* **2009**, *11*, 1275.
[45] A. J. Barnes, *Spectrochim. Acta* **1985**, *41A*, 629.
[46] G. Varsanyi, in *Vibrational Spectra of Benzene Derivatives*, Academic Press, New York, **1969**.
[47] R. Sperline, Y. Song, H. Freiser, *Langmuir* **1994**, *10*, 37.
[48] K. Hanai, M. Yoshifumi, *Spectrochim. Acta Part A* **1993**, *49*, 1131.
[49] M. Hara, S. Nagano, N. Mizosita, T. Seki, *Langmuir* **2007**, *23*, 12350.
[50] M. Hasegawa, T. Matano, Y. Shindo, T. Sugimura, *Macromolecules* **1996**, *29*, 7897.
[51] L. Wang, S.-J. Park, S. H. Lee, Y.-J. Kim, Y.-B. Kook, S.-W. Kuo, R. M. V. Horn, S. Z. D. Cheng, M.-H. Lee, K.-U. Jeong, *Chem. Mater.* **2009**, *21*, 3838.
[52] K.-U. Jeong, A. J. Jing, B. Mansdorf, M. J. Graham, D.-K. Yang, F. W. Harris, S. Z. D. Cheng, *Chem. Mater.* **2007**, *19*, 2921.
[53] J. H. Jung; S.-E. Kim, E. K. Song, K. S. Ha, N. Kim, Y. Cao, C.-C. Tsai, S. Z. D. Cheng, S. H. Lee, K.-U. Jeong, *Chem. Mater.* **2010**, *22*, 4798.
[54] V. R. Horowitz, L. A. Janowitz, A. L. Modic, P. A. Heiney, P. Collings, *Phys. Rev. E* **2005**, *72*, 041710.
[55] A. F. Kostko, B. H. Cipriano, O. A. Pinchuk, L. Ziserman, M. A. Anisimov, D. Danino, S. R. Raghavan, *J. Phys. Chem. B* **2005**, *109*, 19126.
[56] S.-H. Hwang, S.-J. Park, H. Y. Kim, S.-W. Kuo, S. H. Lee, M.-H. Lee, K.-U. Jeong, *J. Phys. Chem. B* **2009**, *113*, 5843.
[57] Standard test method for flim hardness by pencil test, American Society for Testing and Materials, Standard D **1996**, pp 3363.
[58] R. L. McCarley, B. Vaidya, S. Y. Wei, A. F. Smith, A. B. Patel, J. Feng, M. C. Murphy, S. A. Soper, *J. Am. Chem. Soc.* **2005**, *127*, 842.
[59] K. Matsutani, H. Sugisawa, A. Yokota, Y. Furukawa, M. Tasumi, *Appl. Spectrosc.* **1992**, *46*, 560.
[60] T. Nakano, T. Yokoyama, H. Toriumi, *Appl. Spectrosc.* **1993**, *47*, 1354.
[61] C. Ruslim, M. Hashimoto, D. Matsunaga, T. Tamaki, K. Ichimura, *Langmuir* **2004**, *20*, 95.
[62] D. Matsunaga, T. Tamaki, H. Akiyama, K. Ichimura, *Adv. Mater.* **2002**, *14*, 1477.

© 2011 WILEY-VCH Verlag GmbH & Co. KGaA, Weinheim